RESULTS FROM SUPER-KAMIOKANDE

M. NAKAHATA
Kamioka Observatory, ICRR, University of Tokyo

Super-Kamiokande has been taking data since April 1996. Preliminary results on atmospheric neutrinos and solar neutrinos are presented. The results re-confirmed the atmospheric neutrino anomaly and the solar neutrino problem. A possible solution of these problems could be neutrino oscillations.

1 Introduction

Super-Kamiokande was constructed to investigate neutrino oscillations through atmospheric neutrinos and solar neutrinos, and search for nucleon decays with unprecedented sensitivity.

Currently unresolved issues about neutrinos are masses and oscillations. If neutrinos have masses, it gives a strong clue for physics beyond the standard model. Furthermore, neutrinos may have played an important role in astrophysics through dark matter. Although neutrino oscillations are sensitive to only mass differences of neutrino species, much smaller mass ranges can be investigated than direct search experiments. A probability of neutrino oscillations is given by the following formula:

$$P(\nu_\alpha \to \nu_\beta) = sin^2 2\theta sin^2(1.27\frac{L}{E}\Delta m^2),$$

where θ is the mixing angle of neutrinos, L is the distance from a neutrino source to a detector in unit of kilometer, E is the energy of neutrinos in unit of GeV, and Δm^2 is the difference of mass squares in unit of eV^2. As seen in the equation, one needs longer distance and smaller energy of neutrinos for investigating small Δm^2 . The neutrino oscillation experiments with a baseline of sun-to-earth or earth-size, namely solar neutrino and atmospheric neutrino experiments, are best suited for searching for small Δm^2 . The MSW mechanism[1] of solar neutrino oscillations has given a tool to investigate small mixing angle for $\Delta m^2 = 10^{-7} - 10^{-4}$ eV^2 range.

In this report, preliminary results from Super-Kamiokande on atmospheric neutrinos and solar neutrinos are presented.

2 Super-Kamiokande Detector

The Super-Kamiokande is a water Cherenkov detector located in Kamioka mine in Japan. The detector consists of inner and outer detectors. In the

inner-detector, 11,146 photomultiplier tubes(PMT), each 20 inch in diameter, are uniformly placed facing inward on a 0.707 m grid on the entire surface with dimensions 33.8 m in diameter by 36.2 m high, which contains 32,000 metric tons of water. The total photocathod surface area of all PMT's is 40 % of the surface of the inner-detector. A 4π solid-angle outer-detector surrounds the inner-detector. The outer-detector is also a water Cherenkov counter with 1,885 sets consisting of a wavelength shifter plate and an 8 inch PMT. The thickness of the outer-detector is 2 meters. The outer-detector is designed to reduce external gamma-rays from surrounding rocks and tag cosmic-ray muons. The fiducial volume of the detector is defined to be more than 2 m from the detector wall, which amounts to 22 ktons of water. The data taking of Super-Kamiokande was started in April 1996.

The read-out electronics (ATM modules) was designed to detect low energy events without dead-time. When a signal is detected in a PMT, it is held in two analog buffers at the front-end part of the ATM modules, one for pulse height information and another for timing information. The PMT signal is discriminated with a threshold of 0.2 p.e. and a logical signal of 200 nsec width is made, which is called HIT signal. The HIT signals of all PMTs are summed and a HITSUM signal is made. A global trigger of the detector is issued when the HITSUM signal is greater than 29 PMT hits, which corresponds to 5.7 MeV equivalent electron energy. The trigger signal is distributed to all PMT channels and the PMT data in the analog buffers are digitized.

3 Atmospheric Neutrinos

Atmospheric neutrinos are the decay products of hadronic showers produced by primary cosmic ray interactions in the atmosphere. In recent years, the double-ratio of neutrino events classified by lepton types, $R \equiv (\mu/e)_{DATA}/(\mu/e)_{MC}$, has been studied to approximate the atmospheric neutrino flavor ratio ν_μ/ν_e and to cancel uncertainties in the neutrino flux and cross sections. The measurements of R in underground experiments [2] are summarized in Table 1 together with the preliminary results from Super-Kamiokande. The results of NUSEX and Frejus gave R close to one. Results of Kamiokande, IMB, Soudan-II and Super-Kamiokande gave significantly small R value.

Data of 20.1 kt·yr was accumulated in Super-Kamiokande between May 1996 and June 1997. The atmospheric neutrino events are classified into fully contained (FC) events and partially contained (PC) events. The FC events are selected by requiring no hits in outer-detector. The PC events are selected essentially by requiring single outer-detector hit-cluster close to an exit point of the particles observed in the inner-detector. The vertex positions of PC

Experiment	exposure (kt·yr)	events	R
NUSEX	0.74	50	$0.96\ ^{+0.32}_{-0.28}$
Frejus	2.0	200	$1.00 \pm 0.15 \pm 0.08$
Kamiokande sub-GeV	7.7	482	$0.60\ ^{+0.06}_{-0.05} \pm 0.05$
Kamiokande multi-GeV	6/8.2	233	$0.57\ ^{+0.08}_{-0.07} \pm 0.07$
IMB	7.7	610	$0.54 \pm 0.05 \pm 0.11$
Soudan-II	2.83	331	$0.61 \pm 0.14\ ^{+0.05}_{-0.07}$
Super-K sub-GeV	20.1	1453	$0.64 \pm 0.04 \pm 0.05$
Super-K multi-GeV	20.1	444	$0.60 \pm 0.05 \pm 0.05$

Table 1: Measurements of R in atmospheric neutrino experiments.

Ring numbers	DATA(20.1 kt·yr)	Monte Carlo
1 ring	1453	1551.6
e-like	718	593.9
μ-like	735	957.8
2 ring	436	480.5
$\geq$3 ring	97	116.1
Total	1986	2148.3

$$\frac{(\mu/e)_{DATA}}{(\mu/e)_{MC}} = 0.635^{+0.034}_{-0.033}(stat.) \pm 0.053(sys.)$$

Table 2: Summary of sub-GeV events compared with the Monte Carlo simulation.

events are required to be in the fiducial volume. In total, 2591 FC events and 156 PC events were observed in the 20.1 kt·yr data sample. The FC and PC events are sub-divided into sub-GeV and multi-GeV events. Event summaries of them are shown in Table 2 and 3.

The selection of sub-GeV events in the FC sample is that (1) visible energy (E_{vis}) is less than 1.33 GeV, (2) momentum is greater than 100 MeV/c for e-like events and 200 MeV/c for μ-like, and (3) maximum pulse height of a single PMT is less than 200 p.e., which rejects events with a particle stopping very close to the detector wall. The multi-GeV events are required to be $E_{vis} > 1.33$ GeV. The number of sub-GeV and multi-GeV events are 1986 and 605 in the FC sample. Then, the events are analyzed through Cherenkov ring

FC (20.1 kt·yr)	DATA	Monte Carlo
1 ring	288	304.8
e-like	149	120.5
μ-like	139	184.3
2 ring	207	221.0
$\geq$3 ring	110	133.0
Total	605	658.8
PC (18.1 kt·yr)	156	210.7

$$\frac{(\mu/e)_{DATA}}{(\mu/e)_{MC}} = 0.604^{+0.065}_{-0.058}(stat.) \pm 0.067(sys.)$$

Table 3: Summary of multi-GeV events compared with the Monte Carlo simulation.

number counting program and particle identification program. The misidentification probability of the μ/e separation is estimated to be 1% and 2% in the sub-GeV and multi-GeV samples, respectively. The observed number of single ring e-like and μ-like events are 718 (149) and 735 (139) in sub (multi)-GeV data sample. The all PC events are assumed to be μ-like events. The observed events are compared with a Monte Carlo simulation which uses the flux calculation by Honda et al.[3] and a neutrino interaction program based on accelerator neutrino experiments.[4] Nuclear effects, Pauli principle and a mass difference between μ and electron are also taken into account in the Monte Carlo simulation. The results of R obtained by using single ring events are shown in Table 2 and 3. The obtained R is significantly smaller than unity and it reconfirms the results of Kamiokande and IMB results. The momentum distribution of the single ring events are shown in Fig.1 together with the Monte Carlo simulation. The zenith angle distributions of observed e-like and μ-like events are shown in Figure 2. As seen in the figure, the upward-going μ-like events are significantly smaller than the MC expectations. It is seen both in the sub-GeV and multi-GeV samples. A zenith angle dependence of R is shown in Fig.3. R is not only significantly smaller than unity but also distorted with respect to the zenith angle. The distortion of the zenith angle distribution strongly indicates anomaly in the atmospheric neutrinos, because the systematic error of up/down asymmetry of the detector is negligibly small and the shape of the angular distribution cancels various uncertainties in neutrino cross sections, nuclear effects and etc. Possible solution of the anomaly is neutrino oscillations. Using the zenith angle information together with energy information of events, an allowed region of neutrino oscillation parameters is

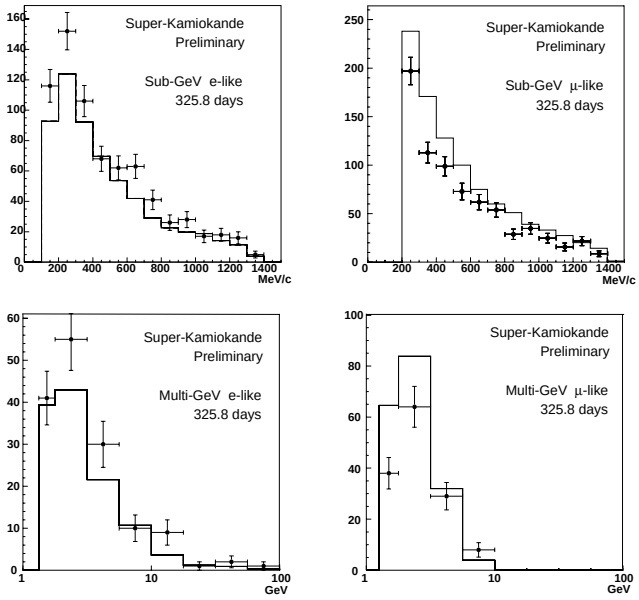

Figure 1: Momentum distribution of single ring events. The obtained data are shown in data points and the solid histograms show the Monte Carlo expectations.

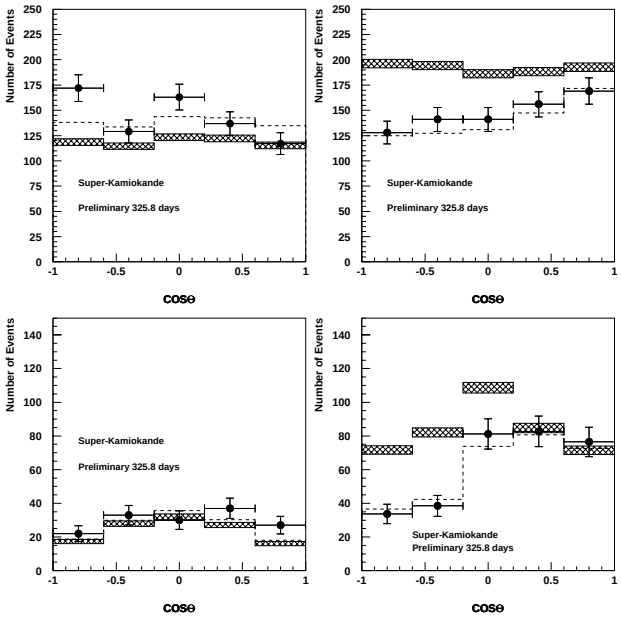

Figure 2: Zenith angle distributions of e-like and μ-like atmospheric neutrino data in Super-Kamiokande. Upper and lower figures are for sub-GeV and multi-GeV data samples, respectively. $cos(\theta)$=1 corresponds to downward-going direction. The hatched bands show MC simulation and dotted histograms show the ones assuming $\nu_\mu \leftrightarrow \nu_\tau$ oscillations with $\Delta m^2 = 5 \times 10^{-3}$ eV^2 and $\sin^2 2\theta$ =1.0.

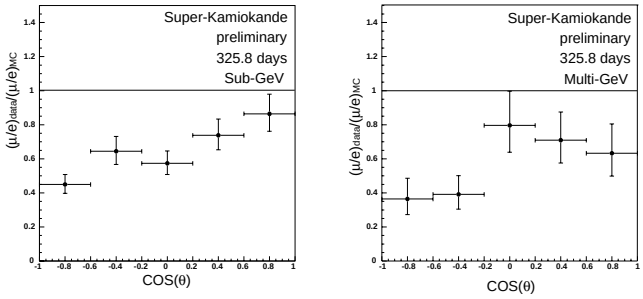

Figure 3: Zenith angle dependence of R.

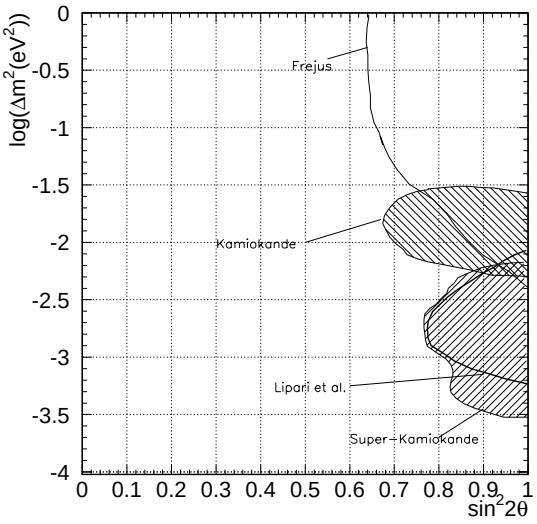

Figure 4: Allowed regions of neutrino oscillation parameters for $\nu_\mu \leftrightarrow \nu_\tau$ oscillations with 90 % C.L. obtained by atmospheric neutrino data in Super-Kamiokande and Kamiokande. The excluded regions by Frejus and IMB are also shown.

obtained as Fig.4. The overlapped allowed regions of Super-Kamiokande and Kamiokande is around $\Delta m^2 = 5 \times 10^{-3}$ eV^2 with large mixing angle. The dotted histograms in Fig.2 show expected zenith angle distributions assuming neutrino oscillations of $\nu_\mu \leftrightarrow \nu_\tau$ with parameters of $\Delta m^2 = 5 \times 10^{-3}$ eV^2 and $\sin^2 2\theta$ =1.0. The neutrino oscillation hypothesis reproduces the observed zenith angle distributions quite well.

4 Solar neutrinos

Results of current solar neutrino experiments[6] and comparison with the standard solar model (SSM) [5] are shown in Table 4. The flux ratio, data/SSM, is 27 % in ν_e^{37}Cl experiment and almost half in Gallium experiments. The νe scattering experiments for ^{8}B neutrinos give data/SSM =$\sim$0.4. A detailed study of the relative difference in the flux ratio indicates that the astrophysical solutions have difficulty in explaining the solar neutrino problem(SNP). [7] An analysis on neutrino oscillations shows that the possible solutions of SNP are a

Experiment	method	flux	Data/SSM(BP95)
^{37}Cl	ν_e^{37}Cl	2.54±0.14±0.14 SNU	0.27±0.02
GALLEX	ν_e^{71}Ga	$69.7\pm6.7^{+3.9}_{-4.5}$ SNU	0.51±0.06
SAGE	ν_e^{71}Ga	73^{+10}_{-11} SNU	$0.53^{+0.07}_{-0.08}$
Kamiokande	νe scat.	(2.80±0.19±0.33)×10^6 /cm^2/sec	0.42±0.06
Super-K.	νe scat.	$(2.37\ ^{+0.06}_{-0.05}\ ^{+0.09}_{-0.07})\times10^6$ /cm^2/sec	$0.358\ ^{+0.017}_{-0.013}$

Table 4: Results of running solar neutrino experiments.

small mixing solution ($\Delta m^2 \sim 0.5\times10^{-5}$ eV^2 and $\sin^2 2\theta \sim 6\times10^{-3}$), a large mixing solution($\Delta m^2 \sim 1\times10^{-5}$ eV^2 and $\sin^2 2\theta \sim 0.6$), and vacuum solution ($\Delta m^2 = 10^{-11} - 10^{-10}$ eV^2 and $\sin^2 2\theta \sim 1$) .[7] The high statistics data of Super-Kamiokande enable us to discuss not only the absolute flux value but also short time variations of the flux, such as day/night effect, and shape of the energy spectrum. Actually, day/night difference of the flux is expected in large mixing solution and a distortion of energy spectrum is expected in the small mixing and the vacuum solutions. Those checks purely depend on properties of neutrinos and are free from any ambiguities in SSM.

Super-Kamiokande has analyzed 374 days' data taken from June 1996 to October 1997. The low energy events which have no outer detector hits and visible energy less than ∼170 MeV (1000 p.e.) are selected at the first stage of data analysis. The vertex positions and directions of the selected events are reconstructed by using the charge and timing data from the hit PMT's. The events with reconstructed vertex in the fiducial volume are selected for the further analysis. At this stage, main source of the background in lower energy range is the radioactivity in the detector, such as Radon in water and gamma-rays from PMT glasses. On the other hand, higher energy range is dominated by spallation background produced by cosmic-ray muon interactions. To reduce lower energy background, additional cuts are applied using an event topology and directionality with respect to the nearest wall from the vertex position. The spallation background is reduced by using timing and spatial correlation with energetic muons. The events thus obtained in the energy range from 6.5 MeV to 20 MeV are used for the solar neutrino analysis.

The Super-Kamiokande detector is calibrated by using an electron linear accelerator (LINAC). It is used to calibrate the absolute energy scale, angular resolution and vertex position resolutions. The LINAC, located ∼13 m away from the Super-Kamiokande detector, injects mono-energetic electrons with a tunable energy ranging from 5 MeV to 16 MeV. The beam is transported into

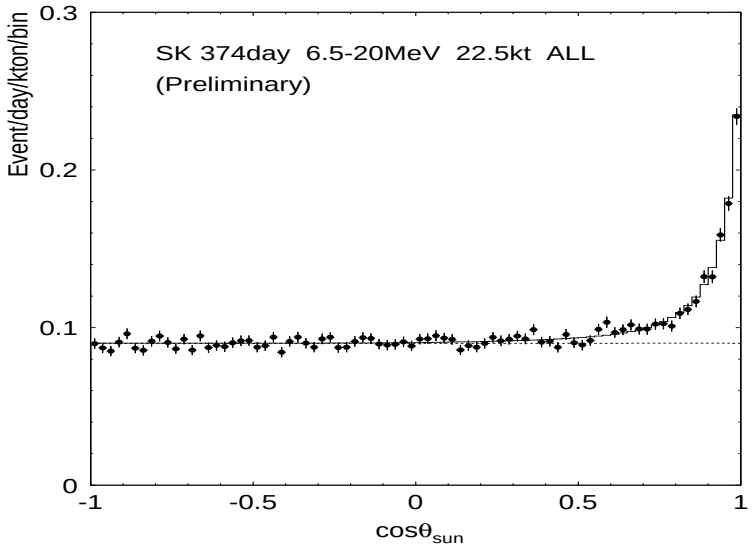

Figure 5: Angular distribution with respect to the direction of the Sun.

the detector through a 10 cm diameter beam pipe, while the beam energy is determined by a system of bending magnets and collimators. The uncertainty of the absolute energy scale is estimated to be ~ 0.45 % at 8 MeV using the LINAC calibration data.

The direction cosine of the events with respect to the direction of the sun ($\cos\theta_{sun}$) is shown in Fig.5. A clear enhancement of signals in the direction of the sun is seen in the angular distribution. The flux obtained by the signals is $(2.37^{+0.06}_{-0.05}\ ^{+0.09}_{-0.07}) \times 10^6$ /cm^2/sec. Comparing the flux with the SSM by Bahcall and Pinsonneault, the flux ratio, data/SSM, is $0.358^{+0.009}_{-0.008}\ ^{+0.014}_{-0.010}$.

The solar neutrino data are sub-divided into day-time and night-time data and flux of each data set is obtained to be $(2.30\pm0.08\ ^{+0.09}_{-0.07}) \times 10^6$ /cm^2/sec for day-time and $(2.44\pm0.08\ ^{+0.10}_{-0.07}) \times 10^6$ /cm^2/sec for night-time. The difference between day and night fluxes is

$$\frac{Day - Night}{Day + Night} = -0.031 \pm 0.024(stat.) \pm 0.014(sys.).$$

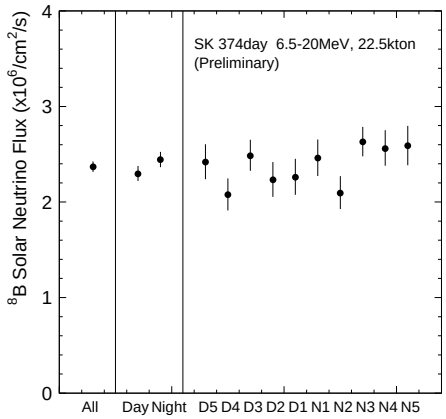

Figure 6: Solar neutrino flux of all data, day and night data, and 5 sub-divided data sets in day and night. D5 and N5 corresponds to downward and upward solar neutrinos, respectively.

The day and night data are further sub-divided into 5 data sets according to the zenith angle of the sun. The flux of each data set is shown in Fig.6. No significant day/night difference nor variation of flux during night-time are seen in the current solar neutrino data. The energy spectrum of recoil electrons from solar neutrino interactions is compared with a prediction from the SSM as shown in Fig.7

Within statistical and systematic errors, the spectrum is consistent with the prediction. However, by reducing these errors by taking more data and perform more precise energy calibration, the Super-Kamiokande is able to discuss the distortion of the energy spectrum in near future.

Excluded regions neutrino oscillation parameters are obtained by using the current analysis of day/night difference and spectral shape as shown in Fig.8. The lower half of the large mixing solution is excluded by the day/night analysis.

5 Conclusions

A preliminary results of 326 days' atmospheric neutrino data is presented. The obtained double ratio, $(\mu/e)_{DATA}/(\mu/e)_{MC}$, is significantly smaller than unity. A strong distortion of zenith angle distribution is observed in μ-like events. The atmospheric neutrino anomaly could be due to neutrino oscillations of $\nu_\mu \leftrightarrow \nu_\tau$

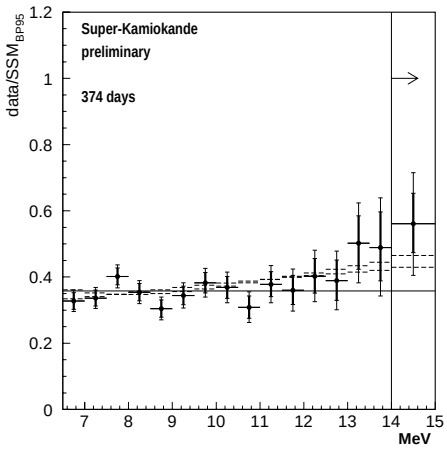

Figure 7: Energy spectrum of recoil electrons normalized by the SSM prediction. Inner error bars are statistical errors and outer bars are systematic errors. Dashed and dotted histograms are the expected spectra of typical small mixing and vacuum solutions, respectively.

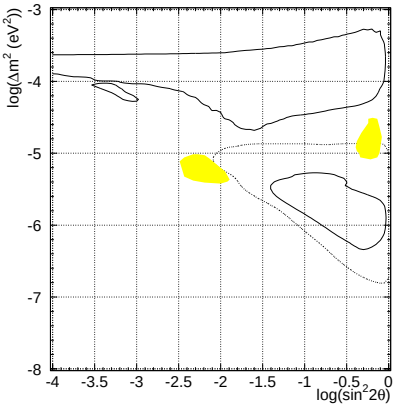

Figure 8: 95 % C.L. excluded regions in MSW solutions. The solid regions are excluded by spectral shape analysis and the dotted region is excluded by the day/night analysis. The shaded regions are large mixing and small mixing solutions given by Hata and Langacker.

with $\Delta m^2 \sim 5 \times 10^{-3}$ eV^2 and $\sin^2 2\theta \sim 1.0$.

Preliminary result of solar neutrino flux obtained by 374 days' data sample is $(2.37^{+0.06}_{-0.05}\ ^{+0.09}_{-0.07}) \times 10^6$ /cm^2/sec, which is 36 % of the prediction from the SSM. No significant day/night difference is observed in the current data sample. A precise energy calibration by LINAC will enable us to discuss the distortion of the energy spectrum in near future.

References

1. L. Wolfenstein, Phys. Rev. D17(1978)2369; S. P. Mikheyev and A. Yu. Smirnov, Nuovo cimento 9C(1986)17; H. A. Bethe, Phys. Rev. Lett. 56(1986)1305.
2. References are in order: M. Aglietta et al., Eourophys. Lett. 8(1989)611; Ch.Berger et al., Phys. Lett. B245(1990)305; K. S. Hirata et al., Phys. Lett. B205(1988)416; K. S. Hirata et al., Phys. Lett. B280(1992)146; R. Becker-Szendy et al., Phys. Rev. D46(1992)3720; W. W. M Allison et al., Phys. Lett. B391(1997)491.
3. M. Honda et al., Phys. Rev. D52(1995)4985.
4. M. Nakahata et al., J. Phys. Soc. Jpn. 55(1986)3786.
5. J. N. Bahcall and M. H. Pinsonneault, Rev. Mod. Phys. 67(1995)781.
6. K. Lande Proceedings of the 17th International Conference on Neutrino Physics and Astrophysics, ed. by K. Enqvist et al., World Scientific(1996)25; W. Hampel et al., Phys. Lett. B357(1996)384; Results of SAGE I+II+III, private communication with V. N. Gavrin; Y. Fukuda et al., Phys. Rev. Lett. 77(1996)1683.
7. N. Hata and P. Langacker, LASSNS-AST 97/29, hep-ph/9705339.